

Thermal Transport by Electrons and Ions in Warm Dense Aluminum: A Combined Density Functional Theory and Deep Potential Study

Qianrui Liu,¹ Junyi Li,² and Mohan Chen^{1, a)}

¹⁾*CAPT, HEDPS, College of Engineering, Peking University, Beijing 100871, P. R. China*

²⁾*School of Computer Science and Technology, Harbin Institute of Technology (Shenzhen), Shenzhen, Guangdong 518055, China*

(Dated: 3 January 2023)

We propose an efficient scheme, which combines density functional theory (DFT) with deep potentials (DP), to systematically study the convergence issues of the computed electronic thermal conductivity of warm dense Al (2.7 g/cm^3 , temperatures ranging from 0.5 to 5.0 eV) with respect to the number of k -points, the number of atoms, the broadening parameter, the exchange-correlation functionals and the pseudopotentials. Furthermore, the ionic thermal conductivity is obtained by the Green-Kubo method in conjunction with DP molecular dynamics simulations, and we study the size effects in affecting the ionic thermal conductivity. This work demonstrates that the proposed method is efficient in evaluating both electronic and ionic thermal conductivities of materials.

^{a)}Electronic mail: mohanchen@pku.edu.cn (Corresponding author)

I. INTRODUCTION

Warm dense matter (WDM) is a state of matter lying between condensed matter and plasma, which consists of strongly coupled ions and partially degenerated electrons. WDM exists in the interior of giant planets^{1,2} or the crust of white dwarf and neutron stars^{3,4} and can be generated through laboratory experiments such as diamond anvil cell,⁵ gas gun^{6,7} and high power lasers.^{7,8} WDM also plays an important role in the inertial confinement fusion (ICF).⁹ In this regard, it is crucial to understand properties of WDM such as the equation of state, optical and transport properties. Due to the lack of experimental data, quantum-mechanics-based simulation methods such as Kohn-Sham density functional theory (KSDFT),^{10,11} orbital-free density functional theory (OFDFT),¹² and path-integral monte carlo¹³⁻¹⁶ have emerged as ideal tools to study WDM.¹⁶⁻²⁰ Thermal conductivity is one of the upmost important properties of warm dense matter. For example, it is widely studied in the modeling the interior structure of planets.²¹⁻²³ It is a key parameter in the hydrodynamic instability growth on the National Ignition Facility capsule design.²⁴ It also plays a key role in simulations of the interactions between laser and a metal target.²⁵ Besides, the thermal conductivity largely affects predictions of ICF implosions in hydrosimulations.²⁶

The thermal conductivity includes both electronic and ionic contributions. The Kubo-Greenwood (KG) formula^{27,28} has been widely applied to study the electronic thermal conductivity κ_e of liquid metals and WDM.^{18,26,29-35} Typically, the κ_e value is averaged over results from several atomic configurations, which are selected from first-principles molecular dynamics (FPMD) simulations. However, it is computationally expensive to perform FPMD simulations for large systems, especially for WDM when the temperatures are high.^{19,33,36,37} Besides, the size effects may substantially affect κ_e , as has been demonstrated in previous works.^{30,33,38} For computations of the ionic thermal conductivity κ_I , we focus on utilizing the Green-Kubo (GK) formula,^{27,39,40} where κ_I is expressed by the heat flux auto-correlation function requiring the energy and the virial tensor of each atom from the molecular dynamics trajectory. Typically, this formula is used with empirical force fields⁴¹⁻⁴³ since traditional DFT methods cannot yield explicit energy for each atom; note that *ab initio* GK formulas for evaluation of κ_I have been proposed in some recent works.⁴⁴⁻⁴⁷ Besides, a long molecular dynamics trajectory may be needed to evaluate κ_I , which poses another challenge issue for DFT simulations.

While current experimental techniques only measure the total thermal conductivity, the first-principles methods have become an ideal tool to separately yield electronic and ionic contributions; however, only a few works that adopt first-principles methods have focused on transport properties by considering both contributions.^{32,48,49} For some metals, the ionic contribution is not important,⁴⁸ but this observation does not hold for all metals such as tungsten.⁴⁹ Besides, the first-principles methods are computationally expensive especially when a large system or a long trajectory is considered. In this regard, the community awaits for an efficient and accurate method that can yield both electronic and ionic thermal conductivities of materials. Herein, with the above KG and GK formulas, we propose a combined DFT and deep potential (DP) method for the purpose and take warm dense Al as an example. The recently developed DP molecular dynamics (DPMD)^{50–52} method learns first-principles data via deep neural networks and yields a highly accurate many-body potential to describe the interactions among atoms. Compared with the traditional DFT, DPMD has a much higher efficiency while keeps the *ab initio* accuracy. In addition, the linear-scaling DPMD can be parallelized to simulate hundreds of millions of atoms.^{53,54} The DP method has been adopted in a variety of applications, such as crystallization of silicon,⁵⁵ high entropy materials,⁵⁶ isotope effects in liquid water,^{57,58} and warm dense matter,^{59,60} etc.

In this work, we demonstrate that the DP method in conjunction with DFT can be adopted to obtain both electronic and ionic thermal conductivities for warm dense Al. We use KSDFE, OFDFT and DPMD to study the electronic and ionic thermal conductivities of warm dense Al at temperatures of 0.5, 1.0 and 5.0 eV with a density of 2.7 g/cm³. The electronic thermal conductivity can be accurately computed via the KG method based on the DPMD trajectories as compared to the FPMD trajectories. Importantly, we systematically investigate the convergence issues such as the number of *k*-points, the number of atoms, the broadening parameter, the exchange-correlation functionals, and the pseudopotentials in affecting the electronic thermal conductivity with the aid of DPMD simulations. Furthermore, the ionic thermal conductivity can be obtained via DPMD and the convergence is studied with different sizes of systems and different lengths of trajectories.

The manuscript is organized as follows. In section II, we briefly introduce KSDFE, OFDFT, and DPMD and the setups of simulations. We also briefly introduce the Kubo-Greenwood formula and the Green-Kubo formula that used in this work. In section III, we first show the computed electronic thermal conductivity from the above three methods.

The convergence issues of the electronic thermal conductivity are then thoroughly discussed. Finally, we show the results of the ionic thermal conductivity of warm dense Al. We conclude our works in Section IV.

II. METHOD

A. Density Functional Theory

The ground-state total energy within the formalism of DFT^{10,11} can be expressed as a functional dependence of the electron density. The Hohenberg-Kohn theorems¹⁰ point out that the electron density which minimizes the total energy is the ground-state density while the energy is the ground-state energy.¹⁰ According to different treatments with the kinetic energy of electrons, two methods appear, i.e., KSDFT¹¹ and OFDFT.¹² The kinetic energy of electron in KSDFT does not include the electron density explicitly but is evaluated from the ground-state wave functions of electrons obtained by the self-consistent iterations. On the other hand, OFDFT approximately denotes the kinetic energy of electrons as an explicit density functional,⁶¹⁻⁶⁵ which enables the direct search for the ground-state density and energy. As a result, KSDFT has a higher accuracy but OFDFT is several orders more efficient than KSDFT, especially for large systems. Besides, Mermin extends DFT to finite temperatures,⁶⁶ which has been widely used to describe electrons in WDM.^{18,29}

We ran 64-atom Born-Oppenheimer molecular dynamics (BOMD) simulations with KSDFT by using the QUANTUM ESPRESSO 5.4 package.⁶⁷ The Perdew-Burke-Ernzerhof (PBE) exchange-correlation (XC) functional⁶⁸ was used. Projector augmented-wave (PAW) potential^{69,70} was adopted with three valence electrons and a cutoff radius of 1.38 Å. The plane wave cutoff energy was set to 20 Ry for temperatures of 0.5 and 1.0 eV and 30 Ry for 5.0 eV. We only used the gamma k -point. Periodic boundary conditions were used. Besides, the Andersen thermostat⁷¹ was employed with the NVT ensemble and the trajectory length was 10 ps with a time step of 1.0 fs.

We also performed 108-atom BOMD simulations with OFDFT by utilizing the PROFESS 3.0 package.⁷² Both PBE⁶⁸ and LDA¹¹ XC functionals were used, in together with the Wang-Teter (WT) KEDF⁶⁵ and the Nosé-Hoover thermostat^{73,74} in the NVT ensemble. We ran OFDFT simulations for 10 ps with a time step of 0.25 fs and the energy cutoff was set to

900 eV. Periodic boundary conditions were utilized.

B. Deep Potential Molecular Dynamics

The DP method^{50–52} learns the dependence of the total energy on the coordinates of atoms in a system and build a deep neural network (DNN) model, which predicts the potential energy and force of each atom. In the training process, the total potential energy E_{tot} is decomposed into energies of different atoms:

$$E_{tot} = \sum_i E_i, \tag{1}$$

where E_i is the potential energy of atom i . In general, for each atom i , the mapping is established through DNN between E_i and the atomic coordinates of its neighboring atoms within a cutoff radius r_c . Specifically, the DNN model consists of the embedding network and the fitting network.⁵⁰ The embedding network imposes constrains to atoms, enabling atomic coordinates to obey the translation, rotation and permutation symmetries. On the other hand, the fitting network maps the atomic coordinates from the embedding network to E_i . Next, the training data are prepared as the total energy and the forces acting on atoms are extracted from the FPMD trajectories. Finally, the parameters of the DNN model are optimized by minimizing the loss function. The resulting DNN-based model can be used to simulate a large system with the efficiency comparable to empirical force fields.

In this work, we adopted the DNN-based models trained from either KSDFT or OFDFT trajectories with the DeePMD-kit package.⁵¹ With the purpose to study the size effects of electronic thermal conductivity, a series of cubic cells consisting of 16, 32, 64, 108, 216 and 256 atoms were simulated for 10 ps with a time step of 0.25 fs. Besides, we ran systems of 16, 32, 64, 108, 256, 1024, 5488, 8192, 10648, 16384, 32000 and 65536 atoms in order to investigate the convergence of ionic thermal conductivity. The length of these trajectories is 500 ps with a time step of 0.25 fs. We employed the Nosé-Hoover thermostat^{73,74} in the NVT ensemble. Periodic boundary conditions were adopted. All of the DPMD simulations were performed by the modified LAMMPS package.⁷⁵

C. Kubo-Greenwood Formula

Electronic thermal conductivity κ_e is calculated by the Onsager coefficients L_{mn} as

$$\kappa_e = \frac{1}{e^2 T} \left(L_{22} - \frac{L_{12}^2}{L_{11}} \right), \quad (2)$$

where T is temperature and e is the charge of electrons, and L_{mn} is obtained by the frequency-dependent Onsager coefficients $L_{mn}(\omega)$ as

$$L_{mn} = \lim_{\omega \rightarrow 0} L_{mn}(\omega). \quad (3)$$

We follow the Kubo-Greenwood formula derived by Holst *et al.*,⁷⁶ and $L_{mn}(\omega)$ takes the form of

$$\begin{aligned} L_{mn}(\omega) &= (-1)^{m+n} \frac{2\pi e^2 \hbar^2}{3m_e^2 \omega \Omega} \\ &\times \sum_{ij\alpha\mathbf{k}} W(\mathbf{k}) \left(\frac{\epsilon_{i\mathbf{k}} + \epsilon_{j\mathbf{k}}}{2} - \mu \right)^{m+n-2} |\langle \Psi_{i\mathbf{k}} | \nabla_\alpha | \Psi_{j\mathbf{k}} \rangle|^2 \\ &\times [f(\epsilon_{i\mathbf{k}}) - f(\epsilon_{j\mathbf{k}})] \delta(\epsilon_{j\mathbf{k}} - \epsilon_{i\mathbf{k}} - \hbar\omega), \end{aligned} \quad (4)$$

where m_e is the mass of electrons, Ω is the volume of cell, $W(\mathbf{k})$ represents the weight of \mathbf{k} points in the Brillouin zone, μ is the chemical potential, $\Psi_{i,\mathbf{k}}$ represents the wave function of the i -th band with the eigenvalue $\epsilon_{i,\mathbf{k}}$ and f being the Fermi-Dirac function. We used the chemical potential μ instead of the enthalpy per atom, which does not affect the results of electronic thermal conductivity in one-component systems.⁷⁶ Note that here we adopted the momentum operator in Eq. (4) instead of the velocity operator, which introduces additional approximations due to the use of non-local pseudopotentials.^{18,34,77-79} However, the non-local errors were demonstrated to be sufficiently small (about 3.3%) for liquid Al,⁷⁸ which are considered to be reasonably small in this work. In future works, we will include the additional term caused by non-local pseudopotentials. We also define the frequency-dependent electronic thermal conductivity as

$$\kappa_e(\omega) = \frac{1}{e^2 T} \left(L_{22}(\omega) - \frac{L_{12}^2(\omega)}{L_{11}(\omega)} \right). \quad (5)$$

In practical usage of the KG method, the delta function in Eq. (4) needs to be broadened. We adopt a Gaussian function²⁹ and the delta function takes the form of

$$\delta(E) = \lim_{\Delta E \rightarrow 0} \frac{1}{\sqrt{2\pi} \Delta E} e^{-\frac{E^2}{2\Delta E^2}}. \quad (6)$$

Here ΔE controls the full width at half maximum (FWHM, denoted as σ) of Gaussian function with the relation of $\sigma \approx 2.3548\Delta E$.

The KG method needs computed eigenvalues and wave functions from DFT solutions of given atomic configurations. In practice, we selected 5-20 atomic configurations from the last 2-ps MD trajectories with a time interval of 0.1 ps. We used both PBE and LDA XC functionals and the associated norm conserving (NC) pseudopotentials in order to test the influences of XC functionals and pseudopotentials on the resulting electronic thermal conductivity. We adopted two NC pseudopotentials for Al, which are referred as PP1 and PP2. The PP1 pseudopotential was generated with the optimized norm-conserving Vanderbilt pseudopotential method via the ONCVSP package.^{80,81} We used 11 valence electrons and a cutoff radius of 0.50 Å. Calculations of κ_e in a 64-atom cell involved 1770, 2100 and 5625 bands at temperatures of 0.5, 1.0 and 5.0 eV, respectively. The PP2 pseudopotential was generated through the PSLibrary package.⁸² We used the Troullier-Martins method⁸³ and the cutoff radius was set to 1.38 Å. We chose 3 valence electrons for each atom. We selected 720, 1100 and 4800 bands for calculations of κ_e at temperatures of 0.5, 1.0 and 5.0 eV, respectively. The plane wave cutoff energies of both pseudopotentials were set to 50 Ry. Generally, the PP1 pseudopotential was used in most cases and the PP2 pseudopotential was only used to compare the effects of different pseudopotentials on κ_e . Fig. 1 shows the computed averaged $\kappa_e(\omega)$ with respect to different numbers of atomic configurations from 108-atom DPMD trajectories at 0.5 and 5.0 eV. The DP model was trained based on the 108-atom OFDFT trajectories using the PBE XC functional. We can see that 20 atomic configurations are enough to converge $\kappa_e(\omega)$. Additionally, $\kappa_e(\omega)$ is easier to converge at the relatively lower temperature of 0.5 eV. Therefore, we chose 20 atomic configurations for cells with 108 atoms or less at all of the three temperatures. For systems with the number of atoms larger than 108, we respectively selected 5 and 10 atomic configurations for temperatures smaller than 5.0 eV and equal to 5.0 eV unless otherwise specified.

D. Green-Kubo Formula

In the DPMD method, the total potential energy of the system is decomposed onto each atom. In this regard, the ionic thermal conductivity can be calculated through the GK

method⁴⁰ with the formula of

$$\kappa_I = \frac{1}{3\Omega k_B T^2} \int_0^{+\infty} \langle \mathbf{J}_q(t) \cdot \mathbf{J}_q(0) \rangle dt, \quad (7)$$

where Ω is the volume of cell, T is temperature, k_B is the Boltzmann constant, $\langle \dots \rangle$ is ensemble average and t is time. \mathbf{J}_q in Eq. (7) is the heat current of a one-component system in the center-of-mass frame which takes the form of

$$\mathbf{J}_q = \sum_{i=1}^N \varepsilon_i \mathbf{v}_i - \frac{1}{2} \sum_{i=1}^N \sum_{j \neq i}^N (\mathbf{v}_i \cdot \mathbf{F}_{ij}) \mathbf{r}_{ij}. \quad (8)$$

Here \mathbf{v}_i is the velocity of the i -th atom, while ε_i is the energy of the i -th atom including ionic kinetic energy and potential energy, where the potential energy is directly obtained by DNN. \mathbf{F}_{ij} is the force acting on the i -th atom due to the presence of the j -th atom with \mathbf{r}_{ij} defined as $\mathbf{r}_i - \mathbf{r}_j$. It is worth mentioning that Eq. (8) is valid for 2-body potentials but yields about 20% error for \mathbf{J}_q when a many-body potential (e.g. the deep potential) is adopted.⁸⁴ Importantly, as will be shown below, the ionic thermal conductivity of warm dense Al is at least two orders of magnitudes smaller than the electronic thermal conductivity counterpart. Therefore, we still consider Eq. (8) as a valid but approximated formula to yield the ionic thermal conductivity of warm dense Al with DPMD. Additionally, we recommend the usage of a more complete formula for those systems whose ionic thermal conductivity is an important part of the total thermal conductivity.

Eq. (7) can also be written as

$$\kappa_I = \int_0^{+\infty} C_J(t) dt, \quad (9)$$

from which the auto-correlation function of heat current is defined as

$$C_J(t) = \frac{1}{3\Omega k_B T^2} \langle \mathbf{J}_q(t) \cdot \mathbf{J}_q(0) \rangle. \quad (10)$$

III. RESULTS

A. Accuracy of DP models

We first performed FPMD simulations of Al based on KSDFE and OFDFT at temperatures of 0.5, 1.0 and 5.0 eV. The PBE XC functional was used and the FPMD trajectory length was 10 ps. The cell contained 64 Al atoms. Two DP models named DP-KS

and DP-OF were trained based on the KSDFE and OFDFE trajectories, respectively. Note that the accuracy of the DP models in describing warm dense Al at the three temperatures have been demonstrated in our previous work,⁵⁹ where we show that DPMD has an excellent accuracy in reproducing structural and dynamical properties including radial distribution functions, static structure factors, and dynamic structure factors.

Here, we first focus on the frequency-dependent Onsager coefficients $L_{mn}(\omega)$. Fig. 2 shows the computed $L_{11}(\omega)$, $L_{12}(\omega)$, and $L_{22}(\omega)$ via different methods at 0.5 eV; $L_{21}(\omega)$ is not illustrated since $L_{21}(\omega) = L_{12}(\omega)$ as derived from Eq. (4). We can see that all of the four methods yield very close $L_{11}(\omega)$ and $L_{22}(\omega)$ except for $L_{12}(\omega)$, where slightly larger differences are found at low frequencies. The main reason is that $L_{12}(\omega)$ is more sensitive to the number of ionic configurations and 20 snapshots are not enough to converge it well. We also test 40 snapshots and the results are improved, as illustrated in Fig. 2(d). However, the resulting electronic thermal conductivity mainly depends on $L_{22}(\omega)$ at temperatures considered in this work and the small differences of $L_{12}(\omega)$ do not affect the computed $\kappa_e(\omega)$, as will be shown next.

The computed frequency-dependent electronic thermal conductivity $\kappa_e(\omega)$ utilizing the abovementioned four different methods are illustrated in Fig. 3. We can see that the OFDFE results agree well with the KSDFE ones, suggesting OFDFE has the same accuracy as KSDFE to yield atomic configurations for subsequent computations of $\kappa_e(\omega)$ using the KG method, even though there are some approximations on the kinetic energy of electrons⁶⁵ and the local pseudopotential⁸⁵ within the framework of OFDFE. Impressively, the DP models trained from FPMD trajectories yield almost identical $\kappa_e(\omega)$ when compared to the DFT results, which proves that the DP models can yield highly accurate atomic configurations for subsequent calculations of $\kappa_e(\omega)$. In conclusion, the input atomic configurations for the calculation of $\kappa_e(\omega)$ can be generated by efficient DPMD models without losing accuracy, which is beneficial for simulating a large number of atoms to mitigate size effects. Although the preparation of the training data in the DPMD model requires additional computational resources, we find running FPMD with a cell consisting of 64 atoms is sufficient to generate reliable DPMD models. Therefore, additional computational costs are saved once larger numbers of atoms are adopted in the linear-scaling DPMD method.⁵⁹

B. Convergence of Electronic Thermal Conductivity

Previous works^{30,33,38} have shown that the electronic thermal conductivity κ_e depends strongly on both the number of k -points and the number of atoms. Additionally, the broadening parameter should be properly chosen in order to yield a meaningful κ_e . Herein, we systematically investigate the above issues by adopting the DPMD model to generate atomic configurations for subsequent calculations of κ_e . The DPMD model was trained from OFDFT-based MD trajectory with the PBE XC functional. By utilizing the snapshots from the DPMD trajectory, we obtain κ_e by using the KG formula. Furthermore, we study the effects of different XC functionals and pseudopotentials in affecting κ_e .

1. Number of k -points

We first investigate the convergence of $\kappa_e(\omega)$ with respect to different k -points. Fig. 4 illustrates an example of warm dense Al in a 64-atom cell at a temperature of 1.0 eV. The k -point meshes were chosen to be $1 \times 1 \times 1$, $2 \times 2 \times 2$, $3 \times 3 \times 3$, and $4 \times 4 \times 4$ in calculations of $\kappa_e(\omega)$. The results show that $\kappa_e(\omega)$ converges when $3 \times 3 \times 3$ k -points are used. In fact, the required number of k -points for convergence of $\kappa_e(\omega)$ varies with different number of atoms and different temperatures. Table I lists the sizes of k -points that are needed to converge $\kappa_e(\omega)$ with numbers of atoms ranging from 16 to 256 at temperatures of 0.5, 1.0 and 5.0 eV. We find that the needed number of k -points exhibits a trend to decrease at higher temperatures. For instance, the needed k -point samplings of a 32-atom cell at temperatures of 0.5, 1.0 and 5.0 eV are $6 \times 6 \times 6$, $5 \times 5 \times 5$ and $3 \times 3 \times 3$, respectively. This can be understood by the fact that the Fermi-Dirac distribution of electrons around the Fermi energy becomes more sharp at low temperatures. Therefore, a dense mesh of k -points is needed to represent the detailed structures around the Fermi surface at low temperatures.

2. Number of atoms

The value of $\kappa_e(\omega)$ converges not only with enough number of k -points but also with sufficient number of atoms in the simulation cell. To demonstrate this point, we plot $\kappa_e(\omega)$ with respect to different numbers of atoms in Fig. 5. For each size of cell, the number of k -points is chosen large enough to converge $\kappa_e(\omega)$, as listed in Table I. We have the

following findings. First, for the temperatures of 0.5, 1.0 and 5.0 eV, we find that a 256-atom system is large enough to converge $\kappa_e(\omega)$. Second, most of $\kappa_e(\omega)$ do not monotonically decrease but have peaks at low frequencies ranging from 0.3 to 0.6 eV. These peaks move towards $\omega=0$ when a larger number of atoms are utilized, and almost disappear in large cells such as the 432-atom cell at 0.5 eV. Similar to previous works,³⁸ this phenomenon is caused by the size effects. Third, $\kappa_e(\omega)$ converges faster with respect to the number of atoms at high temperatures, suggesting that the size effects are less significant at higher temperatures. For example, κ_e of the 16- and 64-atom systems at 0.5 eV are 59.7% (195.5 $\text{Wm}^{-1}\text{K}^{-1}$) and 15.6% (409.3 $\text{Wm}^{-1}\text{K}^{-1}$) lower than the value from a 256-atom system (485.1 $\text{Wm}^{-1}\text{K}^{-1}$). Meanwhile, κ_e of the 16- and 64-atom systems at 5.0 eV are only 47.7% (669.7 $\text{Wm}^{-1}\text{K}^{-1}$) and 7.5% (1182.2 $\text{Wm}^{-1}\text{K}^{-1}$) lower than the value from a 256-atom system (1281.7 $\text{Wm}^{-1}\text{K}^{-1}$).

We perform further analysis to elucidate the origin of size effects in computations of $\kappa_e(\omega)$, which is due to insufficient small energy intervals caused by limited sizes of systems. As Eq. (4) shows, for a given energy interval $\epsilon_{i\mathbf{k}} - \epsilon_{j\mathbf{k}}$ with electronic states of i and j at a specific k point, $\kappa_e(\omega)$ should converge with enough electronic eigenstates; however, Fig. 5 illustrates that the computed $\kappa_e(\omega)$ substantially becomes larger at low frequencies with increased number of atoms in the simulation cell. The results imply that the information of small energy intervals gained from finite-size DFT calculations are insufficient to evaluate $\kappa_e(\omega)$ even when the number of k -points reaches convergence but a small number of atoms is adopted. To clarify this issue, we define an energy interval distribution function (EIDF) as

$$g(E) = \frac{1}{N_p} \sum_{i>j,\mathbf{k}} W(\mathbf{k})\delta(\epsilon_{i\mathbf{k}} - \epsilon_{j\mathbf{k}} - E), \quad (11)$$

where $W(\mathbf{k})$ represents the weights of k -points used in DFT calculations, $\epsilon_{i\mathbf{k}}$ and $\epsilon_{j\mathbf{k}}$ are the eigenvalues and N_p is a normalization factor. We chose warm dense Al systems at temperatures of 0.5 and 5.0 eV with the selected energy intervals computed from the bands occupied by 3s and 3p electrons, which can be identified from density of states (DOS), as illustrated in Fig. 6. The energy intervals satisfy the condition that $E < 1.0$ eV. In addition, we consider the bands within 6.0 and 50.5 eV above the chemical potential μ for temperatures of 0.5 and 5 eV, respectively. The results of $g(E)$ with respect to different numbers of atoms ranging from 16 to 432 atoms are illustrated in Fig. 7. The EIDF $g(E)$ becomes larger for

small E as the number of atoms increases and converges when the number of atoms reaches 256 for both cases at 0.5 and 5.0 eV. The increase of $g(E)$ at small E implies that more energy eigenvalues that have close values appear in a larger cell with more atoms. In other words, because of the finite number of atoms used in the simulation cell, the energy levels are discretized to some extent, resulting in the lack of energy intervals especially for those small values. Particularly, these small energy intervals are of significant importance in evaluating $\kappa_e(\omega)$ when $\omega \rightarrow 0$ as shown in Eq. (4).

3. Broadening Parameter

The FWHM broadening parameter σ that appears in the $\delta(E)$ function in Eq. (6) substantially affects the resulting electronic thermal conductivity $\kappa_e(\omega)$ when $\omega \rightarrow 0$. We therefore investigate the choices of σ in influencing the computed $\kappa_e(\omega)$ by analyzing the EIDF $g(E)$. Taking Al at 0.5 eV as an example, we plot in Fig. 8 both $g(E)$ and $\kappa_e(\omega)$ of a 256-atom cell, which is large enough to converge $g(E)$ or $\kappa_e(\omega)$ as demonstrated above. When the broadening effect is small ($\sigma=0.01$ eV), $g(E)$ and $\kappa_e(\omega)$ decrease dramatically below 0.2 eV, which is caused by the discrete band energies. Thus, a suitable σ needs to be chosen to compensate the discrete band energies. For instance, the value of $g(E)$ at $E=0$ increases from 0.22 eV^{-1} ($\sigma=0.01$ eV) to 0.99 eV^{-1} ($\sigma=0.4$ eV). However, $g(E)$ becomes saturated if a too large σ is applied, resulting in overcorrected $\kappa_e(\omega)$ that the curve at frequencies lower than 0.6 eV decreases. Therefore, in order to compensate the discrete band energies and avoid overcorrection at the same time, we choose σ to be 0.4 eV for warm dense Al at all of the temperatures considered in this work. It is worth mentioning that a majority of works including this work treat the broadening parameter as an adjustable variable to yield a better characterized line of frequency-dependent thermal conductivity.^{18,29–31,33,34,38} Even though some physical criteria have been proposed,⁸⁶ the choice of the adjustable variable is still inconclusive. In this work, we choose the adjustable parameter in terms of sufficient small energy intervals, which are possible when a sufficiently large supercell is used in DFT calculations. The κ_e at zero frequency is obtained by the linear extrapolation and illustrated in Fig. 9.

4. Exchange-correlation functionals

We study the influences of LDA and PBE XC functionals on the computed $\kappa_e(\omega)$ by first validating the atomic configurations generated by FPMD simulations. Specifically, atomic configurations were chosen from two 256-atom DPMD trajectories, which were generated by two DP models trained from OFDFT with the LDA and PBE XC functionals. We then adopted the KG method by using the PP1 pseudopotentials generated with the same XC functional, and yielded κ_e at temperatures of 0.5, 1.0, and 5.0 eV. As shown in Fig. 9 and listed in Table. II, the κ_e values obtained from the PBE XC functional are 485.1, 764.1 and 1281.7 $\text{Wm}^{-1}\text{K}^{-1}$ at temperatures of 0.5, 1.0 and 5.0 eV, respectively, while the κ_e values from the LDA XC functional are 1.6% lower (477.3 $\text{Wm}^{-1}\text{K}^{-1}$), 1.3% higher (773.8 $\text{Wm}^{-1}\text{K}^{-1}$) and 2.8% lower (1246.4 $\text{Wm}^{-1}\text{K}^{-1}$) than those of PBE at 0.5, 1.0 and 5.0 eV respectively. Therefore, we conclude that the LDA XC functional yields almost the same κ_e values as PBE. Note that a recent work⁸⁷ adopted the HSE XC functional and showed some differences in electronic thermal and electrical conductivities of warm dense Al as compared with those from the PBE XC functional.

5. Pseudopotentials

We investigate how norm-conserving pseudopotentials affect the computed electronic thermal conductivity κ_e . First of all, Fig. 6 shows DOS of two types of pseudopotentials (PP1 and PP2) at temperatures of 0.5 and 5.0 eV, where we see that the two pseudopotentials yield similar DOS of $3s3p$ electrons. Next, Fig. 9 illustrates the computed κ_e from two types of pseudopotentials and those computed data from Knyazev *et al.*,³¹ Vlcěk *et al.*³⁴ and Witte *et al.*,⁸⁷ as well as the experimental data from McKelvey *et al.*⁸⁸ Besides, κ_e from two types of pseudopotentials are also listed in Table.II.

We have the following findings. First, the DP-OF results agree reasonably well with the DP-KS ones, as have been previously shown in Fig. 3. For example, DP-KS with the PP1 pseudopotential and the PBE XC functional yields $\kappa_e=466.5 \text{ Wm}^{-1}\text{K}^{-1}$ at 0.5 eV, which is 3.8% lower than that of DP-OF (485.1 $\text{Wm}^{-1}\text{K}^{-1}$) at the same temperature and the relative difference decreases to 1.9% at 5.0 eV. The above results imply that the OFDFT is suitable to study the electronic thermal conductivity of warm dense Al ranging from 0.5

to 5.0 eV. Second, our calculations with the PP1 and PP2 pseudopotentials yield similar κ_e values of around 480 and 770 $\text{Wm}^{-1}\text{K}^{-1}$ at 0.5 and 1.0 eV, respectively. The results are consistent with those from Knyazev *et al.*, Vlček *et al.* and Witte *et al.* However, the κ_e values from the two pseudopotentials at 5.0 eV deviate. For instance, the result of DP-OF (PBE) with the PP2 pseudopotential is 1604.6 $\text{Wm}^{-1}\text{K}^{-1}$ while the result with the PP1 pseudopotential is only 1281.7 $\text{Wm}^{-1}\text{K}^{-1}$, which is 20.1% lower than the former one. The κ_e values from PP1 are close to those from Witte *et al.*, while the κ_e values from PP2 are consistent with the Knyazev *et al.* data. Note that Witte *et al.* utilized a PAW potential with 11 valence electrons and the PBE XC functional, while Knyazev *et al.* adopted an ultrasoft pseudopotential with 3 valence electrons and the LDA XC functional. It is also worth mentioning that a 64-atom cell is utilized in the work by Witte *et al.* while a 256-atom cell is used in the work by Knyazev *et al.* In this regard, the size effects may exist in the previous one according to our analysis. In general, both values of electronic thermal conductivity lie within the experimental data of McKelvey *et al.* Even so, our results demonstrate that different pseudopotentials may substantially affect the results of κ_e at high temperatures. One possible reason that causes the deviation of κ_e at 5.0 eV is the number of electrons included in the pseudopotentials. However, it is also possible that the deviation comes from the fact that the non-local potential correction^{77,78} in Eq. (4) is ignored. Therefore, non-local corrections have to be considered when calculating the conductivity via the Kubo-Greenwood formula which is subject of future work.

C. Ionic Thermal Conductivity

The ionic thermal conductivity of warm dense Al can be evaluated by the GK formula since the atomic energies are available in the DPMD method. However, the computed ionic thermal conductivity may be affected by trajectory length and system size. In this regard, we study the convergence of the ionic thermal conductivity with respect to different lengths of trajectories and system sizes. We first test the convergence of the auto-correlation function $C_J(t)$ in Eq. (10) with respect to different lengths of trajectories and the results are shown in Fig. 10. A 10648-atom Al system was adopted with four different lengths of trajectories, i.e., 25, 125, 250, and 500 ps, and the DPMD model was trained from OFDFT with the PBE XC functional at a temperature of 0.5 eV. As illustrated in Fig. 10, the $C_J(t)$

curves abruptly decay within the first 0.1 ps and oscillate with respect to time t . We notice that the oscillations are largely affected by the length of simulation time. For example, $C_J(t)$ obtained from the 25-ps trajectory exhibits substantially larger oscillations than the other three trajectories, and the convergence is better achieved when the 250-ps trajectory is adopted. The above results suggest that in order to yield converged $C_J(t)$ for warm dense Al, a few hundreds of ps are required even for a system with more than ten thousand atoms, which is beyond the capability of FPMD simulations but can be realized by DPMD simulations.

Next, we run 12 different sizes of cells ranging from 16 to 65536 atoms for 500 ps to check the size effects on ionic thermal conductivity, and the results are illustrated in Fig. 11. Since $C_J(t)$ cannot strictly reach zero, a truncation of the correlation time t is applied to the integration of $C_J(t)$ in Eq. (9). In practice, we choose multiple truncations of t ranging from 0.5 to 1.5 ps and computed the error bars with the maximum and minimum integral values, which are also shown in Fig. 11. We find that the ionic thermal conductivity increases with larger system sizes ranging from 16- to 1024 atoms at all of the three temperatures considered for warm dense Al. Next, the ionic thermal conductivity begins to oscillate until the largest system size adopted (65536 atoms). In this regard, we conclude that at least a 1024-atom system should be adopted and a better converged ionic thermal conductivity can be obtained if a larger size of system is used. A 65536-atom cell is utilized to compute the ionic thermal conductivity and the results are in Table II. The ionic thermal conductivity of warm dense Al is around 1-2 $\text{Wm}^{-1}\text{K}^{-1}$, which is more than two orders of magnitudes smaller than the electronic thermal conductivity counterpart. Additionally, both PBE and LDA XC functionals yield similar values for the ionic thermal conductivity.

IV. CONCLUSIONS

We propose a method that combines DPMD and DFT to calculate both electronic and ionic thermal conductivities of materials, and the DP models are trained from DFT-based MD trajectories. The resulting DP models accurately reproduce the properties as compared to those from DFT. In addition, the DP models can be utilized to efficiently simulate a large cell consisting of hundreds of atoms, which largely mitigate the size effects caused by periodic boundary conditions. Next, by using the atomic configurations from DPMD trajectories,

one can use the eigenvalues and eigenstates of a given system obtained from DFT solutions, and adopt the Kubo-Greenwood formula to compute the electronic thermal conductivity. In addition, the DP models yield atomic energies, which are not available in the traditional DFT method. By using the atomic energies to evaluate ionic thermal conductivity, both electronic and ionic contributions to the thermal conductivity can be obtained for a given material.

We took warm dense Al as an example and thoroughly studied its thermal conductivity. Expensive FPMD simulations of large systems can be replaced by DPMD simulations with much smaller computational resources. We first computed the temperature-dependent electronic thermal conductivities of warm dense Al from 0.5 to 5.0 eV at a density of 2.7 g/cm³ with snapshots from OFDFT, KSDFE and DPMD, and the three methods yielded almost the same results, demonstrating that the DPMD method owns similar accuracy as FPMD simulations. We then systematically investigated the convergence issues with respect to the number of k -points, the number of atoms, the broadening parameter, the exchange-correlation functionals, and the pseudopotentials. A 256-atom system was found to be large enough to converge the electronic thermal conductivity. The broadening parameter was chosen to be 0.4 eV according to our analysis of the energy interval distribution function. We found both LDA and PBE XC functionals yielded similar results for the electronic thermal conductivity. However, the choices of pseudopotentials may substantially affect the resulting electronic thermal conductivity. Furthermore, we also computed the ionic thermal conductivity with DPMD and the GK method, and investigated the convergence issues with respect to trajectory length and system size. We found the ionic thermal conductivity of warm dense Al is much smaller than its electronic thermal conductivity. In summary, the DPMD method provides a promising accuracy and efficiency in studying both electronic and ionic thermal conductivity of warm dense Al and should be considered for future work on modeling transport properties of WDM.

ACKNOWLEDGMENTS

This work was Supported by the Strategic Priority Research Program of Chinese Academy of Sciences Grant No. XDC01040100. The work of M. C. is supported by the National Science Foundation of China under Grant No. 12074007. The numerical simulations were performed on the High Performance Computing Platform of CAPT.

REFERENCES

- ¹T. Guillot, “Interiors of giant planets inside and outside the solar system,” *Science* **286**, 72–77 (1999).
- ²N. Nettelmann, A. Becker, B. Holst, *et al.*, “Jupiter models with improved *ab initio* hydrogen equation of state (H-REOS. 2),” *The Astrophysical Journal* **750**, 52 (2012).
- ³F. Wesemael, H. M. Van Horn, M. P. Savedoff, *et al.*, “Atmospheres for hot, high-gravity stars. I-Pure hydrogen models,” *Astrophysical Journal Supplement Series* **43**, 159 (1980).
- ⁴J. Daligault and S. Gupta, “Electron-ion scattering in dense multi-component plasmas: Application to the outer crust of an accreting neutron star,” *The Astrophysical Journal* **703**, 994–1011 (2009).
- ⁵P. Loubeyre, R. LeToullec, D. Hausermann, *et al.*, “X-ray diffraction and equation of state of hydrogen at megabar pressures,” *Nature* **383**, 702–704 (1996).
- ⁶S. T. Weir, A. C. Mitchell, and W. J. Nellis, “Metallization of fluid molecular hydrogen at 140 Gpa (1.4 Mbar),” *Phys. Rev. Lett.* **76**, 1860–1863 (1996).
- ⁷W. J. Nellis, “Dynamic compression of materials: metallization of fluid hydrogen at high pressures,” *Reports on Progress in Physics* **69**, 1479–1580 (2006).
- ⁸R. Cauble, L. B. Da Silva, T. S. Perry, *et al.*, “Absolute measurements of the equations of state of low-Z materials in the multi-Mbar regime using laser-driven shocks,” *Physics of Plasmas* **4**, 1857–1861 (1997).
- ⁹J. Lindl, “Development of the indirect-drive approach to inertial confinement fusion and the target physics basis for ignition and gain,” *Physics of Plasmas* **2**, 3933–4024 (1995).
- ¹⁰P. Hohenberg and W. Kohn, “Inhomogeneous electron gas,” *Phys. Rev.* **136**, 864B (1964).
- ¹¹W. Kohn and L. J. Sham, “Self-consistent equations including exchange and correlation effects,” *Phys. Rev.* **140**, 1133A (1965).

- ¹²Y. A. Wang and E. A. Carter, “Orbital-free kinetic-energy density functional theory,” in *Theoretical Methods in Condensed Phase Chemistry* (Springer, 2002) pp. 117–184.
- ¹³E. L. Pollock and D. M. Ceperley, “Simulation of quantum many-body systems by path-integral methods,” *Phys. Rev. B* **30**, 2555–2568 (1984).
- ¹⁴D. M. Ceperley and E. L. Pollock, “Path-integral computation of the low-temperature properties of liquid ^4He ,” *Phys. Rev. Lett.* **56**, 351–354 (1986).
- ¹⁵E. W. Brown, B. K. Clark, J. L. DuBois, *et al.*, “Path-integral monte carlo simulation of the warm dense homogeneous electron gas,” *Phys. Rev. Lett.* **110**, 146405 (2013).
- ¹⁶B. Militzer and K. P. Driver, “Development of path integral Monte Carlo simulations with localized nodal surfaces for second-row elements,” *Phys. Rev. Lett.* **115**, 176403 (2015).
- ¹⁷B. Holst, R. Redmer, and M. P. Desjarlais, “Thermophysical properties of warm dense hydrogen using quantum molecular dynamics simulations,” *Phys. Rev. B* **77**, 184201 (2008).
- ¹⁸V. Recoules and J.-P. Crocombette, “*Ab initio* determination of electrical and thermal conductivity of liquid aluminum,” *Phys. Rev. B* **72**, 104202 (2005).
- ¹⁹C. Wang and P. Zhang, “Wide range equation of state for fluid hydrogen from density functional theory,” *Physics of Plasmas* **20**, 092703 (2013).
- ²⁰M. Bonitz, T. Dornheim, Z. A. Moldabekov, *et al.*, “*Ab initio* simulation of warm dense matter,” *Physics of Plasmas* **27**, 042710 (2020).
- ²¹W. B. Hubbard, “Thermal structure of jupiter,” *The Astrophysical Journal* **152**, 745–754 (1968).
- ²²R. W. Siegfried and S. C. Solomon, “Mercury: Internal structure and thermal evolution,” *Icarus* **23**, 192 – 205 (1974).
- ²³S. Labrosse, “Thermal and magnetic evolution of the earth’s core,” *Physics of the Earth and Planetary Interiors* **140**, 127 – 143 (2003), *geophysical and Geochemical Evolution of the Deep Earth*.
- ²⁴M. M. Marinak, S. W. Haan, T. R. Dittrich, *et al.*, “A comparison of three-dimensional multimode hydrodynamic instability growth on various National Ignition Facility capsule designs with HYDRA simulations,” *Physics of Plasmas* **5**, 1125–1132 (1998).
- ²⁵D. S. Ivanov and L. V. Zhigilei, “Combined atomistic-continuum modeling of short-pulse laser melting and disintegration of metal films,” *Phys. Rev. B* **68**, 064114 (2003).

- ²⁶S. X. Hu, L. A. Collins, T. R. Boehly, *et al.*, “First-principles thermal conductivity of warm-dense deuterium plasmas for inertial confinement fusion applications,” *Phys. Rev. E* **89**, 043105 (2014).
- ²⁷R. Kubo, “Statistical-mechanical theory of irreversible processes. I. General theory and simple applications to magnetic and conduction problems,” *Journal of the Physical Society of Japan* **12**, 570–586 (1957).
- ²⁸D. A. Greenwood, “The boltzmann equation in the theory of electrical conduction in metals,” *Proceedings of the Physical Society* **71**, 585–596 (1958).
- ²⁹M. P. Desjarlais, J. D. Kress, and L. A. Collins, “Electrical conductivity for warm, dense aluminum plasmas and liquids,” *Phys. Rev. E* **66**, 025401 (2002).
- ³⁰D. Knyazev and P. Levashov, “*Ab initio* calculation of transport and optical properties of aluminum: Influence of simulation parameters,” *Computational Materials Science* **79**, 817 – 829 (2013).
- ³¹D. V. Knyazev and P. R. Levashov, “Transport and optical properties of warm dense aluminum in the two-temperature regime: *Ab initio* calculation and semiempirical approximation,” *Physics of Plasmas* **21**, 073302 (2014).
- ³²M. French, A. Becker, W. Lorenzen, *et al.*, “*Ab initio* simulations for material properties along the jupiter adiabat,” *The Astrophysical Journal Supplement Series* **202**, 5 (2012).
- ³³F. Lambert, V. Recoules, A. Decoster, *et al.*, “On the transport coefficients of hydrogen in the inertial confinement fusion regime,” *Physics of Plasmas* **18**, 056306 (2011).
- ³⁴V. Vlček, N. De Koker, and G. Steinle-Neumann, “Electrical and thermal conductivity of Al liquid at high pressures and temperatures from *ab initio* computations,” *Phys. Rev. B* **85**, 184201 (2012).
- ³⁵C. E. Starrett, J. Clérouin, V. Recoules, *et al.*, “Average atom transport properties for pure and mixed species in the hot and warm dense matter regimes,” *Physics of Plasmas* **19**, 102709 (2012).
- ³⁶S. X. Hu, B. Militzer, V. N. Goncharov, *et al.*, “Strong coupling and degeneracy effects in inertial confinement fusion implosions,” *Phys. Rev. Lett.* **104**, 235003 (2010).
- ³⁷D. Sheppard, J. D. Kress, S. Crockett, *et al.*, “Combining Kohn-Sham and orbital-free density-functional theory for Hugoniot calculations to extreme pressures,” *Phys. Rev. E* **90**, 063314 (2014).

- ³⁸M. Pozzo, M. P. Desjarlais, and D. Alfè, “Electrical and thermal conductivity of liquid sodium from first-principles calculations,” *Phys. Rev. B* **84**, 054203 (2011).
- ³⁹M. S. Green, “Markoff random processes and the statistical mechanics of time-dependent phenomena. II. Irreversible processes in fluids,” *The Journal of Chemical Physics* **22**, 398–413 (1954).
- ⁴⁰D. A. McQuarrie, “Statistical mechanics,” (Harpercollins College Div, 1976) pp. 520–521.
- ⁴¹T. Kawamura, Y. Kangawa, and K. Kakimoto, “Investigation of thermal conductivity of gan by molecular dynamics,” *Journal of Crystal Growth* **284**, 197 – 202 (2005).
- ⁴²F. Taherkhani and H. Rezania, “Temperature and size dependency of thermal conductivity of aluminum nanocluster,” *Journal of Nanoparticle Research* **14**, 1222 (2012).
- ⁴³W. K. Kim, J. H. Shim, and M. Kaviani, “Thermophysical properties of liquid UO_2 , ZrO_2 and corium by molecular dynamics and predictive models,” *Journal of Nuclear Materials* **491**, 126 – 137 (2017).
- ⁴⁴C. Carbogno, R. Ramprasad, and M. Scheffler, “*Ab initio* Green-Kubo approach for the thermal conductivity of solids,” *Phys. Rev. L* **118**, 175901 (2017).
- ⁴⁵A. Marcolongo, P. Umari, and S. Baroni, “Microscopic theory and quantum simulation of atomic heat transport,” *Nature Physics* **12**, 80–84 (2016).
- ⁴⁶J. Kang and L.-W. Wang, “First-principles Green-Kubo method for thermal conductivity calculations,” *Phys. Rev. B* **96**, 020302 (2017).
- ⁴⁷M. French, “Thermal conductivity of dissociating water—an ab initio study,” *New Journal of Physics* **21**, 023007 (2019).
- ⁴⁸A. Jain and A. J. H. McGaughey, “Thermal transport by phonons and electrons in aluminum, silver, and gold from first principles,” *Phys. Rev. B* **93**, 081206 (2016).
- ⁴⁹Y. Chen, J. Ma, and W. Li, “Understanding the thermal conductivity and Lorenz number in tungsten from first principles,” *Phys. Rev. B* **99**, 020305 (2019).
- ⁵⁰L. Zhang, J. Han, H. Wang, *et al.*, “End-to-end symmetry preserving inter-atomic potential energy model for finite and extended systems,” in *Advances in Neural Information Processing Systems* (Curran Associates Inc., 2018) pp. 4436–4446.
- ⁵¹H. Wang, L. Zhang, J. Han, *et al.*, “DeePMD-kit: A deep learning package for many-body potential energy representation and molecular dynamics,” *Computer Physics Communications* **228**, 178–184 (2018).

- ⁵²L. Zhang, J. Han, H. Wang, *et al.*, “Deep potential molecular dynamics: A scalable model with the accuracy of quantum mechanics,” *Physical Review Letter* **120**, 143001 (2018).
- ⁵³W. Jia, H. Wang, M. Chen, D. Lu, L. Lin, R. Car, W. E, and L. Zhang, “Pushing the limit of molecular dynamics with *ab initio* accuracy to 100 million atoms with machine learning,” in *Proceedings of the International Conference for High Performance Computing, Networking, Storage and Analysis*, SC ’20 (IEEE Press, 2020).
- ⁵⁴D. Lu, H. Wang, M. Chen, L. Lin, R. Car, W. E, W. Jia, and L. Zhang, “86 pflops deep potential molecular dynamics simulation of 100 million atoms with *ab initio* accuracy,” *Computer Physics Communications* **259**, 107624 (2021).
- ⁵⁵L. Bonati and M. Parrinello, “Silicon liquid structure and crystal nucleation from *ab initio* deep metadynamics,” *Phys. Rev. L* **121**, 265701 (2018).
- ⁵⁶F.-Z. Dai, B. Wen, Y. Sun, *et al.*, “Theoretical prediction on thermal and mechanical properties of high entropy (Zr_{0.2}Hf_{0.2}Ti_{0.2}Nb_{0.2}Ta_{0.2})_c by deep learning potential,” *Journal of Materials Science & Technology* **43**, 168 – 174 (2020).
- ⁵⁷H.-Y. Ko, L. Zhang, B. Santra, *et al.*, “Isotope effects in liquid water via deep potential molecular dynamics,” *Molecular Physics* **117**, 3269–3281 (2019).
- ⁵⁸J. Xu, C. Zhang, L. Zhang, M. Chen, B. Santra, and X. Wu, “Isotope effects in molecular structures and electronic properties of liquid water via deep potential molecular dynamics based on the scan functional,” *Phys. Rev. B* **102**, 214113 (2020).
- ⁵⁹Q. Liu, D. Lu, and M. Chen, “Structure and dynamics of warm dense aluminum: a molecular dynamics study with density functional theory and deep potential,” *Journal of Physics: Condensed Matter* **32**, 144002 (2020).
- ⁶⁰Y. Zhang, C. Gao, Q. Liu, *et al.*, “Warm dense matter simulation via electron temperature dependent deep potential molecular dynamics,” *Physics of Plasmas* **27**, 122704 (2020).
- ⁶¹L. H. Thomas, “The calculation of atomic fields,” *Mathematical Proceedings of the Cambridge Philosophical Society* **23**, 542–548 (1927).
- ⁶²E. Fermi, “Un metodo statistico per la determinazione di alcune proprieta dell’atome,” *Rend. Accad. Naz. Lincei* **6**, 32 (1927).
- ⁶³E. Fermi, “Eine statistische methode zur bestimmung einiger eigenschaften des atoms und ihre anwendung auf die theorie des periodischen systems der elemente,” *Zeitschrift für Physik* **48**, 73–79 (1928).

- ⁶⁴C. v. Weizsäcker, “Zur theorie der kernmassen,” *Zeitschrift für Physik A Hadrons and Nuclei* **96**, 431–458 (1935).
- ⁶⁵L.-W. Wang and M. P. Teter, “Kinetic-energy functional of the electron density,” *Physical Review B* **45**, 13196 (1992).
- ⁶⁶N. D. Mermin, “Thermal properties of the inhomogeneous electron gas,” *Physical Review* **137**, A1441 (1965).
- ⁶⁷P. Giannozzi, O. Andreussi, T. Brumme, *et al.*, “Advanced capabilities for materials modelling with Quantum ESPRESSO,” *Journal of Physics: Condensed Matter* **29**, 465901 (2017).
- ⁶⁸J. P. Perdew, K. Burke, and M. Ernzerhof, “Generalized gradient approximation made simple,” *Physical Review Letters* **77**, 3865 (1996).
- ⁶⁹P. E. Blöchl, “Projector augmented-wave method,” *Physical Review B* **50**, 17953 (1994).
- ⁷⁰N. Holzwarth, A. Tackett, and G. Matthews, “A Projector Augmented Wave (PAW) code for electronic structure calculations, Part I: atompaw for generating atom-centered functions,” *Computer Physics Communications* **135**, 329–347 (2001).
- ⁷¹H. C. Andersen, “Molecular dynamics simulations at constant pressure and/or temperature,” *Journal of Chemical Physics* **72**, 2384–2393 (1980).
- ⁷²M. Chen, J. Xia, C. Huang, *et al.*, “Introducing PROFESS 3.0: An advanced program for orbital-free density functional theory molecular dynamics simulations.” *Computer Physics Communications* **190**, 228–230 (2015).
- ⁷³S. Nosé, “A unified formulation of the constant temperature molecular dynamics methods,” *Journal of Chemical Physics* **81**, 511–519 (1984).
- ⁷⁴W. G. Hoover, “Canonical dynamics: Equilibrium phase-space distributions.” *Phys Rev A Gen Phys* **31**, 1695–1697 (1985).
- ⁷⁵S. Plimpton, “Fast parallel algorithms for short-range molecular dynamics,” *Journal of Computational Physics* **117**, 1–19 (1995).
- ⁷⁶B. Holst, M. French, and R. Redmer, “Electronic transport coefficients from *ab initio* simulations and application to dense liquid hydrogen,” *Phys. Rev. B* **83**, 235120 (2011).
- ⁷⁷A. J. Read and R. J. Needs, “Calculation of optical matrix elements with nonlocal pseudopotentials,” *Phys. Rev. B* **44**, 13071–13073 (1991).
- ⁷⁸F. Knider, J. Hugel, and A. V. Postnikov, “*Ab initio* calculation of dc resistivity in liquid Al, Na and Pb,” *Journal of Physics: Condensed Matter* **19**, 196105 (2007).

- ⁷⁹M. French and R. Redmer, “Electronic transport in partially ionized water plasmas,” *Physics of Plasmas* **24**, 092306 (2017).
- ⁸⁰D. R. Hamann, “Optimized norm-conserving Vanderbilt pseudopotentials,” *Phys. Rev. B* **88**, 085117 (2013).
- ⁸¹D. R. Hamann, “Erratum: Optimized norm-conserving Vanderbilt pseudopotentials [Phys. Rev. B 88, 085117 (2013)],” *Phys. Rev. B* **95**, 239906 (2017).
- ⁸²A. Dal Corso, “Pseudopotentials periodic table: From H to Pu,” *Computational Materials Science* **95**, 337 – 350 (2014).
- ⁸³N. Troullier and J. L. Martins, “Efficient pseudopotentials for plane-wave calculations,” *Phys. Rev. B* **43**, 1993–2006 (1991).
- ⁸⁴P. Boone, H. Babaei, and C. E. Wilmer, “Heat flux for many-body interactions: Corrections to lammmps,” *Journal of Chemical Theory and Computation* **15**, 5579–5587 (2019).
- ⁸⁵C. Huang and E. A. Carter, “Transferable local pseudopotentials for magnesium, aluminum and silicon,” *Physical Chemistry Chemical Physics* **10**, 7109–7120 (2008).
- ⁸⁶D. Kang, S. Zhang, Y. Hou, C. Gao, C. Meng, J. Zeng, and J. Yuan, “Thermally driven fermi glass states in warm dense matter: Effects on terahertz and direct-current conductivities,” *Physics of Plasmas* **26**, 092701 (2019).
- ⁸⁷B. B. L. Witte, P. Sperling, M. French, *et al.*, “Observations of non-linear plasmon damping in dense plasmas,” *Physics of Plasmas* **25**, 056901 (2018).
- ⁸⁸A. McKelvey, G. Kemp, P. Sterne, *et al.*, “Thermal conductivity measurements of proton-heated warm dense aluminum,” *Scientific Reports* **7**, 1–10 (2017).

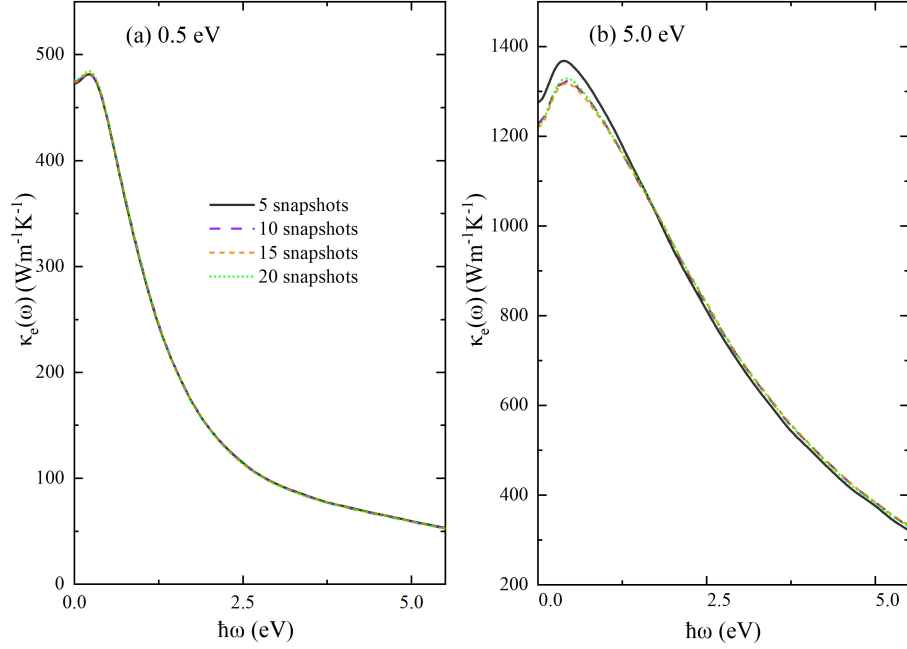


FIG. 1. (Color online) Convergence of frequency-dependent electronic thermal conductivity $\kappa_e(\omega)$ of Al with respect to the number of atomic configurations (snapshots) selected from DPMD trajectories. The temperatures are set to (a) 0.5 and (b) 5.0 eV. The number of snapshots used together with the Kubo-Greenwood formula (the broadening parameter is set to 0.4 eV) is shown with different lines. The DP model is trained from the OFDFT trajectories using the PBE exchange-correlation functional. The simulation cell contains 108 atoms.

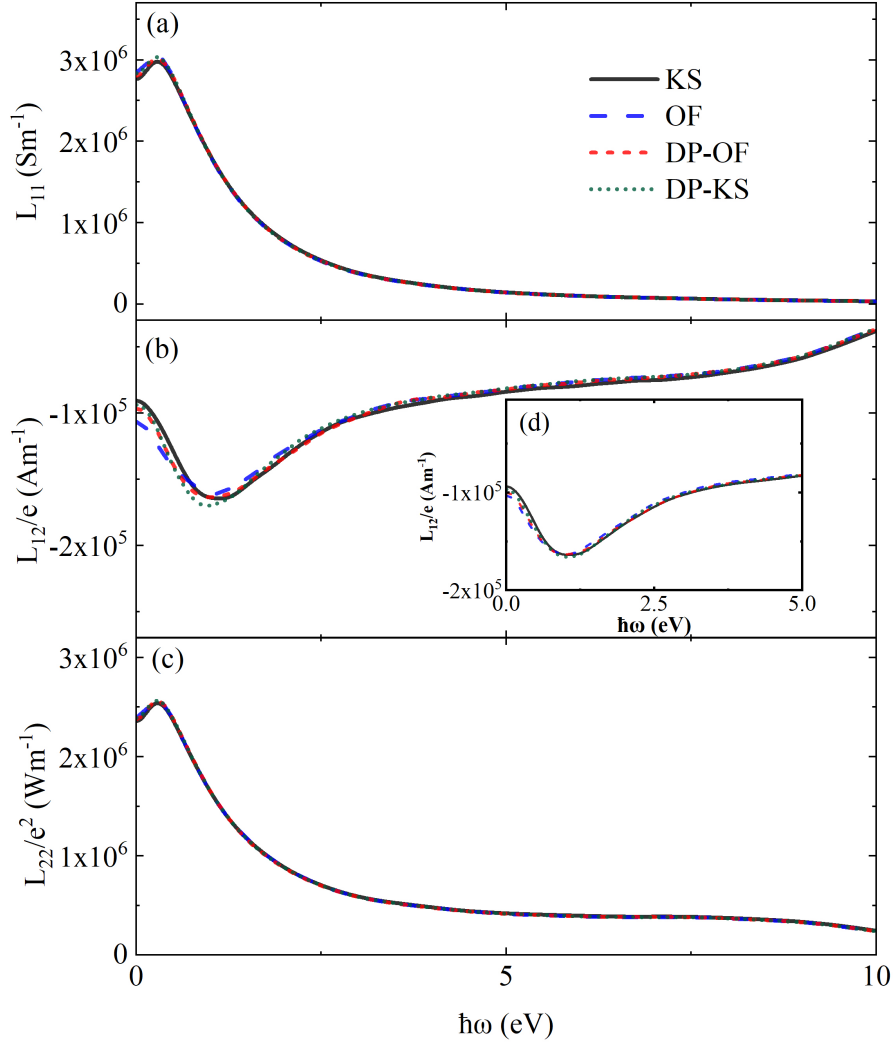


FIG. 2. (Color online) Frequency-dependent Onsager kinetic coefficients (a) L_{11} , (b) L_{12} , and (c) L_{22} of Al at a temperature of 0.5 eV as computed from KS, OF, DP-KS and DP-OF methods. DP-KS and DP-OF refer to the DP models trained from OFDFT and KSDFT molecular dynamics trajectories, respectively. The broadening parameter used in the Kubo-Greenwood method is set to 0.4 eV. The simulation cell contains 64 Al atoms.

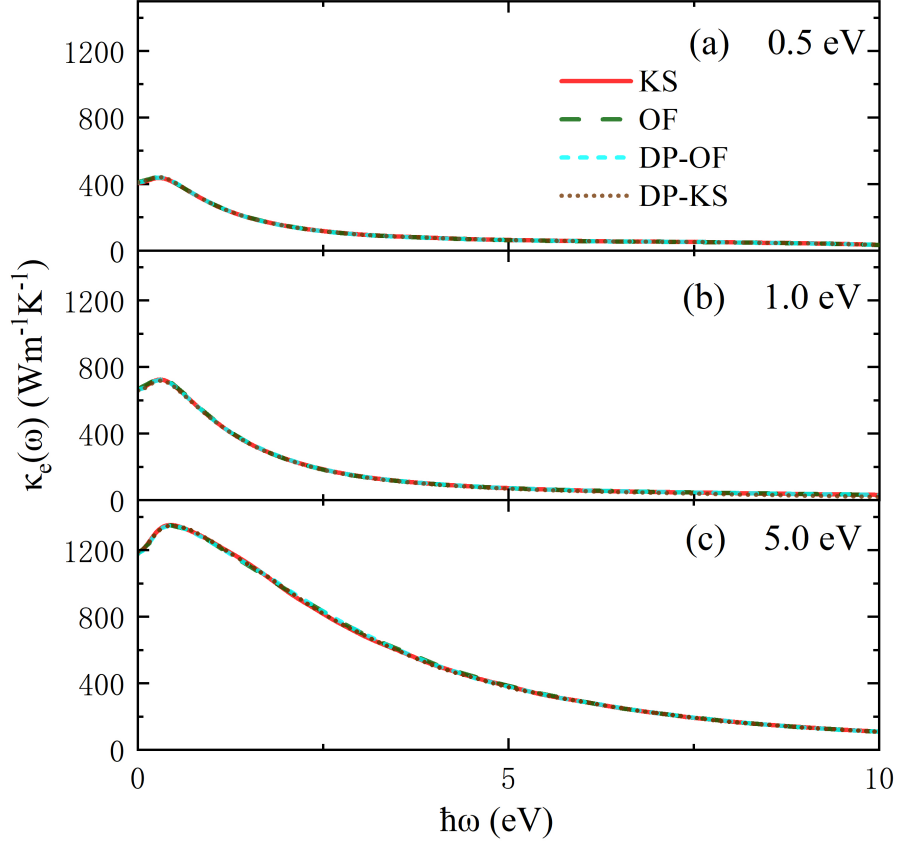


FIG. 3. (Color online) Frequency-dependent electronic thermal conductivity $\kappa_e(\omega)$ as computed from the Kubo-Greenwood method (the broadening parameter is set to 0.4 eV) with snapshots from KS, OF, DP-KS and DP-OF molecular dynamics trajectories. The temperatures are (a) 0.5, (b) 1.0 and (c) 5.0 eV. DP-KS and DP-OF refer to the DP models trained from OFDFT and KSDFT molecular dynamics trajectories, respectively. The cell contains 64 Al atoms.

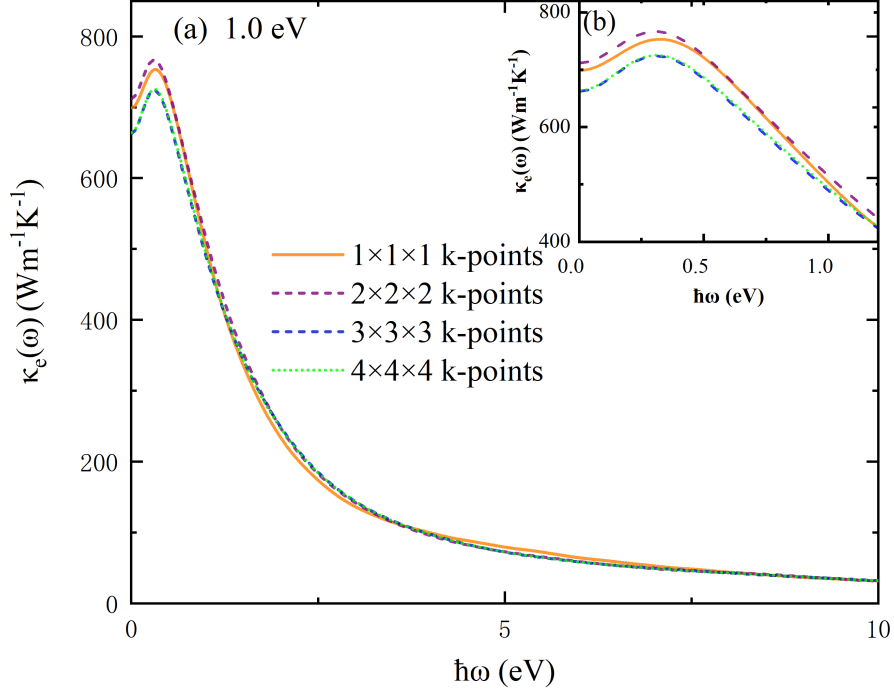


FIG. 4. (Color online) Convergence of frequency-dependent electronic thermal conductivity $\kappa_e(\omega)$ of Al with respect to the number of k -points. The temperature is set to 1.0 eV. The k -point samplings utilized with the Kubo-Greenwood method (the broadening parameter is set to 0.4 eV) are chosen from $1 \times 1 \times 1$ to $4 \times 4 \times 4$. The DP model is trained from the OFDFT trajectories using the PBE exchange-correlation functional. The cell consists of 64 atoms.

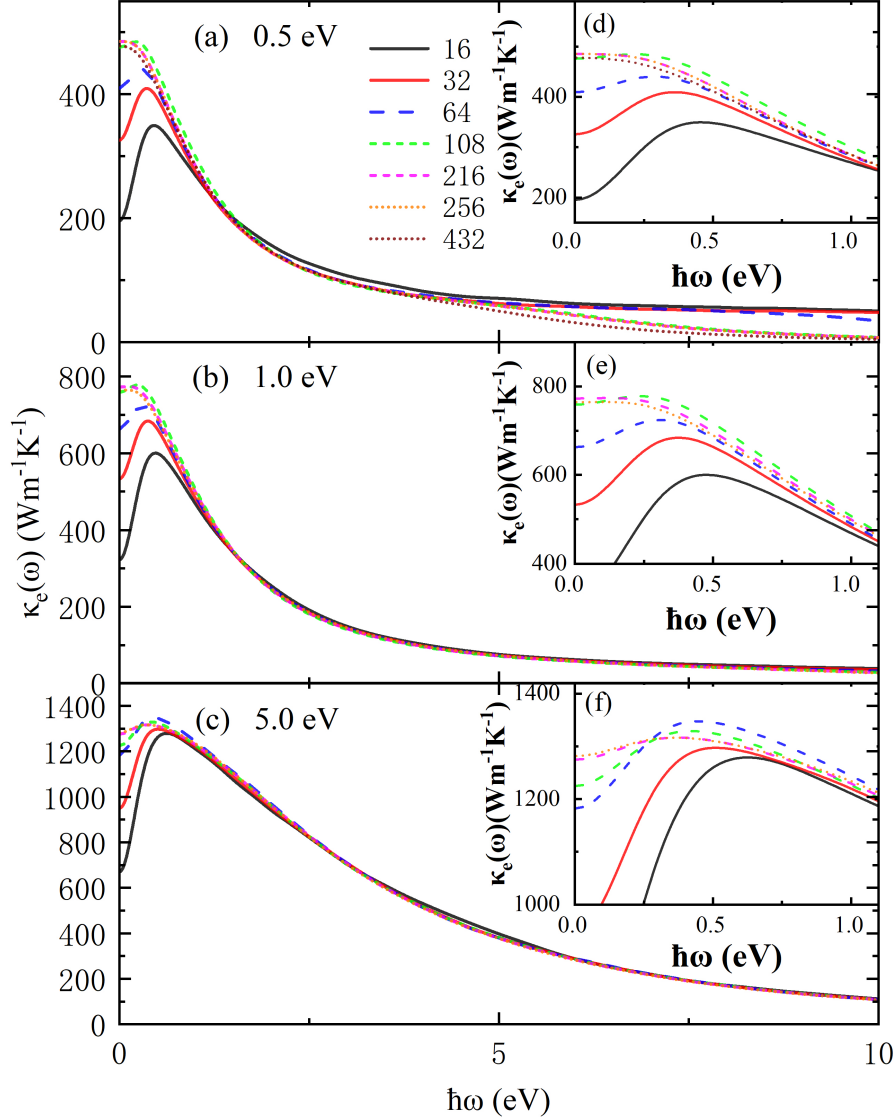


FIG. 5. (Color online) Convergence of the electronic thermal conductivity $\kappa_e(\omega)$ with respect to the number of atoms (from 16 to 432 atoms) in the simulation cell. The temperatures are set to (a) 0.5, (b) 1.0 and (c) 5.0 eV. (d-f) illustrate the peaks in (a-c), respectively. For the temperature of 0.5 eV, two 432-atom snapshots with $2 \times 2 \times 2$ k -points are chosen to test the convergence of $\kappa_e(\omega)$. The DP model is trained from the OFDFT trajectories using the PBE exchange-correlation functional. The broadening parameter is set to 0.4 eV.

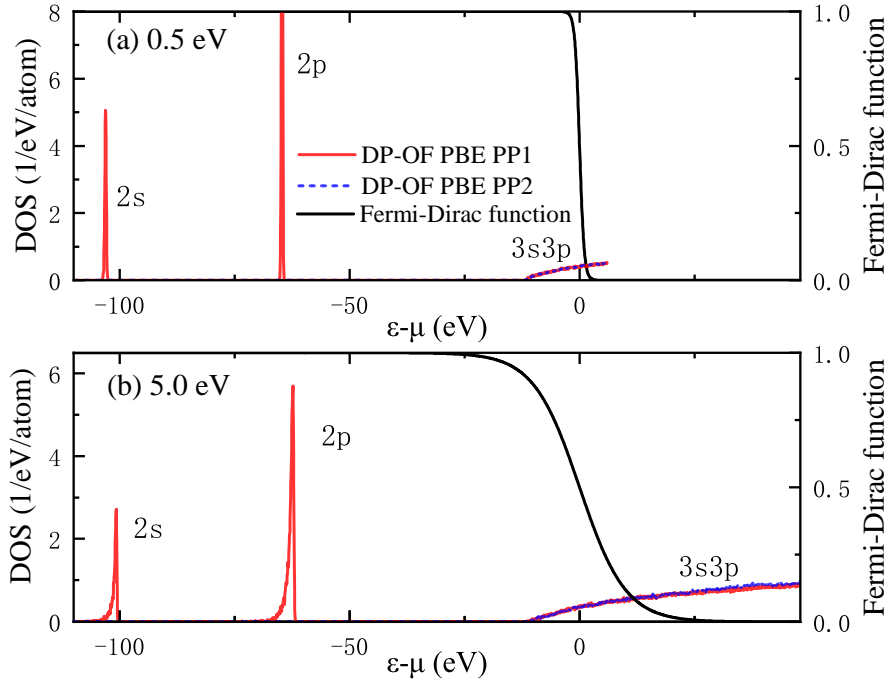


FIG. 6. (Color online) Density of states of a 256-atom cell at temperatures of (a) 0.5 and (b) 5.0 eV. The Fermi-Dirac function at the same temperature is plotted with a black solid line. The DP-OF model refers to the DP model trained from OFDFT molecular dynamics trajectory.

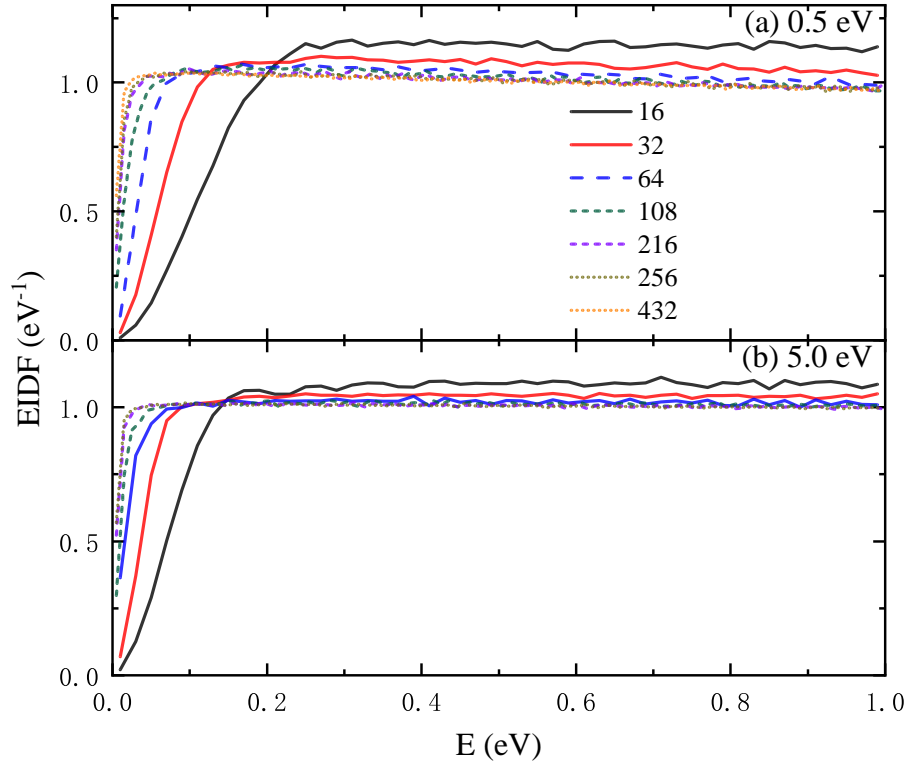


FIG. 7. (Color online) Energy interval distribution function of different cells at (a) 0.5 eV and (b) 5.0 eV. The bands within 6.0 and 50.5 eV above the chemical potential μ are considered for temperatures of 0.5 and 5 eV, respectively. Different lines refer to different numbers of atoms (from 16 to 432 atoms) in the simulation cell. The DP model is trained from the OFDFT trajectories using the PBE exchange-correlation functional.

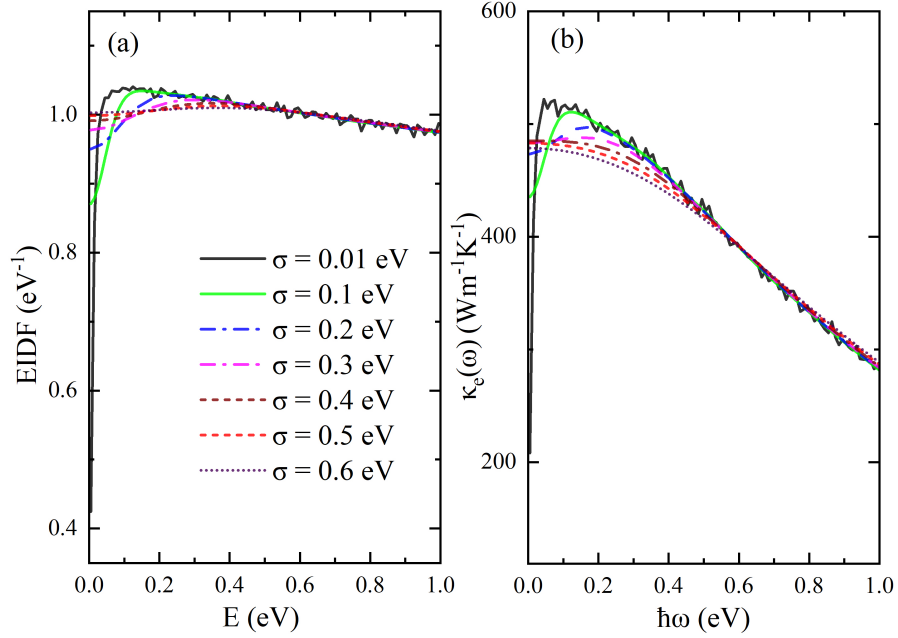


FIG. 8. (Color online) (a) Energy interval distribution function and (b) electronic thermal conductivities of a 256-atom cell at 0.5 eV. The snapshots are from DPMD simulations. The DPMD model is trained from OFDFT trajectories with the PBE exchange-correlation functional. Different lines indicate different broadening parameter σ .

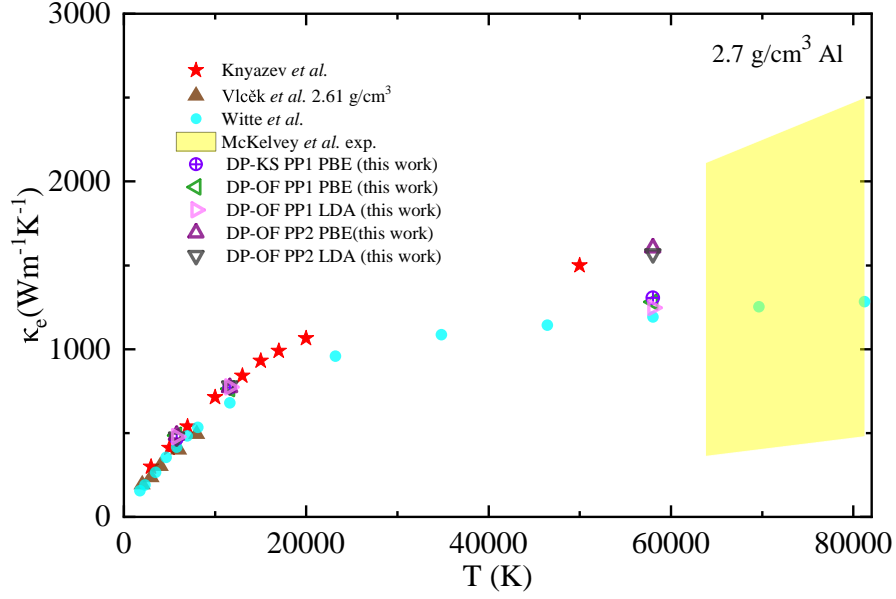


FIG. 9. (Color online) Electronic thermal conductivities κ_e of warm dense Al. DP-KS and DP-OF refer to the DPMD models that trained from KSDFT and OFDFT, respectively. Atomic configurations are generated from DP-KS and DP-OF models. The broadening parameter is set to 0.4 eV. Note that non-local corrections have been neglected in this study. Results from Knyazev *et al.*,³¹ Vlcěk *et al.*³⁴ and Witte *et al.*,⁸⁷ as well as the experimental results from McKelvey *et al.*⁸⁸ are shown for comparison.

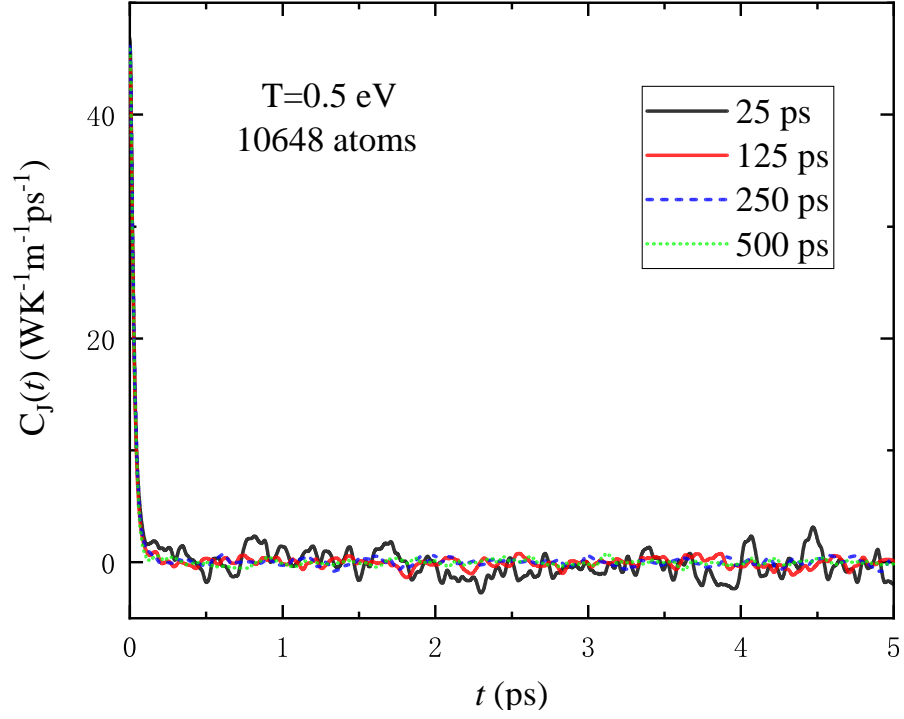


FIG. 10. (Color online) Auto-correlation function of heat current $C_J(t)$ evaluated from different lengths of DPMD trajectories, i.e., 25, 125, 250 and 500 ps. The number of Al atoms in the cell is 10684 and the temperature is $T=0.5$ eV. The DPMD model was trained from OFDFT with the PBE exchange-correlation functional.

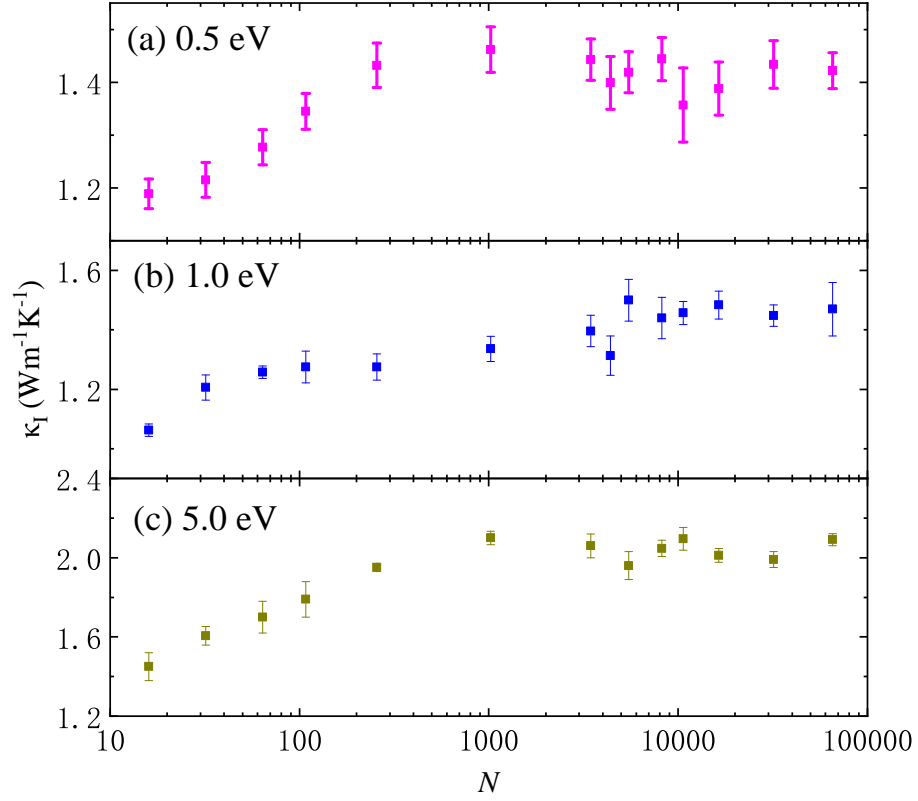


FIG. 11. (Color online) Computed ionic thermal conductivity of warm dense Al at (a) 0.5 eV, (b) 1.0 eV and (c) 5.0 eV with different sizes of systems. The number of atoms N in different cells are 16, 32, 64, 108, 256, 1024, 5488, 8192, 10648, 16384, 32000 and 65536. The results are obtained through DPMD trained from OFDFT with the PBE XC functional.

TABLE I. Sizes of k -points that adopted in KSDFE calculations to converge the electronic thermal conductivity of Al with different number of atoms (N) in the simulation cell at temperatures of 0.5, 1.0 and 5.0 eV.

N	0.5 eV	1.0 eV	5.0 eV
16	$8 \times 8 \times 8$	$7 \times 7 \times 7$	$3 \times 3 \times 3$
32	$6 \times 6 \times 6$	$5 \times 5 \times 5$	$3 \times 3 \times 3$
64	$3 \times 3 \times 3$	$3 \times 3 \times 3$	$1 \times 1 \times 1$
108	$2 \times 2 \times 2$	$2 \times 2 \times 2$	$1 \times 1 \times 1$
216	$2 \times 2 \times 2$	$2 \times 2 \times 2$	$1 \times 1 \times 1$
256	$2 \times 2 \times 2$	$2 \times 2 \times 2$	$1 \times 1 \times 1$
432	$2 \times 2 \times 2$	N/A	N/A

TABLE II. Electronic thermal conductivity κ_e ($\text{Wm}^{-1}\text{K}^{-1}$) and ionic thermal conductivity κ_I ($\text{Wm}^{-1}\text{K}^{-1}$) at temperatures T of 0.5, 1.0 and 5.0 eV. The results are computed from the DP-KS and DP-OF molecular dynamics trajectories. DP-KS and DP-OF refer to the DP models trained from KSDFT and OFDFT molecular dynamics trajectories, respectively.

	T	$\kappa_e(\text{PP1})$	$\kappa_e(\text{PP2})$	κ_I
	0.5 eV	485.1	486.6	1.422±0.034
DP-OF (PBE)	1.0 eV	764.1	772.3	1.469±0.086
	5.0 eV	1281.7	1604.6	2.091±0.031
	0.5 eV	477.3	475.6	1.394±0.047
DP-OF (LDA)	1.0 eV	773.8	779.0	1.318±0.032
	5.0 eV	1246.4	1568.5	2.141±0.051
	0.5 eV	466.5		1.419±0.038
DP-KS (PBE)	1.0 eV	771.0		1.393±0.066
	5.0 eV	1305.8		2.075±0.066